Density-Driven Instabilities of Variable-Viscosity Miscible Fluids in a Capillary Tube

ECKART MEIBURG, SURYA H. VANAPARTHY, MATTHIAS D. PAYR, AND DIRK WILHELM

Department of Mechanical and Environmental Engineering, University of California, Santa Barbara, California, USA

ABSTRACT: A linear stability analysis is presented for variable-viscosity miscible fluids in an unstable configuration; that is, a heavier fluid placed above a lighter one in a vertically oriented capillary tube. The initial interface thickness is treated as a parameter to the problem. The analysis is based on the three-dimensional Stokes equations, coupled to a convection-diffusion equation for the concentration field, in cylindrical coordinates. When both fluids have identical viscosities, the dispersion relations show that for all values of the governing parameters the three-dimensional mode with an azimuthal wave number of one represents the most unstable disturbance. The stability results also indicate the existence of a critical Rayleigh number of about 920, below which all perturbations are stable. For the variable viscosity case, the growth rate does not depend on which of the two fluids is more viscous. For every parameter combination the maximum of the eigenfunctions tends to shift toward the less viscous fluid. With increasing mobility ratio, the instability is damped uniformly. We observe a crossover of the most unstable mode from azimuthal to axisymmetric perturbations for Rayleigh numbers greater than 10^5 and high mobility ratios. Hence, the damping influence is much stronger on the three-dimensional mode than the corresponding axisymmetric mode for large Rayleigh numbers. For a fixed mobility ratio, similar to the constant viscosity case, the growth rates are seen to reach a plateau for Rayleigh numbers in excess of 10^6. At higher mobility ratios, interestingly, the largest growth rates and unstable wave numbers are obtained for intermediate interface thicknesses. This demonstrates that, for variable viscosities, thicker interfaces can be more unstable than their thinner counterparts, which is in contrast to the constant viscosity result where growth rate was seen to decline monotonically with increasing interface thickness.

KEYWORDS: density-driven instabilities; variable viscosity; miscible fluids; capillary tube

INTRODUCTION

The capillary tube represents one of the fundamental configurations historically employed in investigations of interfacial phenomena and diffusive effects in the region of contact between two fluids. Both hydrodynamic stability problems and

Address for correspondence: Eckart Meiburg, Department of Mechanical and Environmental Engineering, University of California, Santa Barbara, CA 93106, USA. Voice/fax: 805-893-5278.
meiburg@engineering.ucsb.edu

Ann. N.Y. Acad. Sci. **1027: 383–402 (2004).**
doi: 10.1196/annals.1324.032

displacement processes have been studied extensively in the above geometry. Hales[1] was among the first to address the stability of an unstably stratified, variable density fluid mixture with a constant density gradient in a vertically oriented capillary tube, in the absence of any net flow through the tube. He found that a stable equilibrium is possible, as long as the density gradient does not exceed a certain critical value. Taylor[2] devised a simple experiment to obtain this critical gradient of density that he argued could be used in order to determine the diffusion coefficient of a fluid pair, see also recent related experimental work.[3] Wooding[4] took an analytical approach to the stability problem for a constant density gradient in a capillary tube. He observed that the three-dimensional mode $\beta = 1$, where β denotes the azimuthal wave number, represents the most unstable disturbance. The above analysis was extended[5] to base states involving density profiles that vary sinusoidally in the vertical direction or deviate from a constant value only in a central layer of small vertical extent. This work confirmed that $\beta = 1$ represents the most unstable mode for the uniform density gradient. Without proof, it was assumed that this also holds for the case of sinusoidally varying density. All of the above investigations were limited to cases in which viscosity variations are absent. To our knowledge, the situation that can be realized most easily in an experiment, namely that of a relatively thin, miscible interface formed by placing a heavier fluid above a lighter one in a capillary tube, has not yet been addressed from a stability theoretical point of view. Variable viscosity influence on density driven instability is an interesting extension. This is the configuration analyzed in the investigation we report here.

The presence of a net flow through the tube complicates the situation considerably. Other investigations[6,7] discussed the fractional amount of viscous fluid left behind on the wall of a tube when it is expelled by an inviscid fluid with which it is immiscible as a function of a suitably defined capillary number *Ca*. Density effects were deemed unimportant in these studies. Numerical calculations for this case,[8] showed very good agreement with the experimental observations. This classical work has recently been extended to finite viscosity ratios.[9] Petitjeans and Maworthy[10] and Chen and Meiburg[11] analyzed the corresponding miscible problem both experimentally and computationally, based on the Stokes equations (see also the related experiments in Ref. 12). In these flows, a cutoff length is set by diffusive effects rather than surface tension, so that in some sense, a Péclet number *Pe* takes the place of *Ca*. The above authors also address the role of density differences by conducting experiments and simulations in vertical tubes. Substantial differences between the experiments and the numerical data are observed at small values of *Pe*, in that a quasisteady finger emerges for significantly smaller values of *Pe* in the simulations, as compared to the experiments. This raises the question as to whether nonconventional, so-called Korteweg stresses[13,14] or divergence effects, can be important, an issue that has been addressed elsewhere.[15] A particularly striking finding was reported in the follow-up experiments of Kuang *et al.*[16] In a vertical capillary tube without net flow, these authors observe that the sharp interface formed by placing a heavier, more viscous silicone oil above a lighter and less viscous one leads to an interfacial instability with an azimuthal wave number $\beta = 1$. However, when a small upward net flow was applied to this gravitationally unstable base state, the interface evolved in an axisymmetric fashion, rather than exhibiting an azimuthal instability mode.

As a first step, in the present work, we perform the linear stability analysis of the density-driven instability for variable-viscosity miscible fluids in a capillary tube. The analysis is based on the three-dimensional Stokes equations, and it proceeds along similar lines as our recent investigation for the corresponding situation in a Hele–Shaw cell,[17,18] as well as the related experiments and nonlinear simulations.[19] Introduction of a net flow will be the next step. It is to be seen if the aforementioned experimental observation reflects an effect of the net flow within the linear framework of the stability problem, or if it represents a nonlinear effect.

The paper is organized as follows: initially the physical problem, the governing equations, and the relevant dimensionless parameters are described in more detail. Next, the linearization is described for both axisymmetric and azimuthal perturbations, and the numerical procedure for solving the resulting eigenvalue problem is outlined. Subsequently, the results of the stability analysis are presented in the form of dispersion relations and associated information for the two cases of identical and different viscosity fluids. Finally, we summarize our main conclusions.

PHYSICAL PROBLEM

Governing Equations

We consider the situation of variable-viscosity miscible fluids in an unstable configuration; that is, a heavier fluid placed above a lighter one in a vertically oriented capillary tube, as shown in FIGURE 1. We assume a suitably defined Reynolds number to be small, so that the motion is governed by the three-dimensional Stokes equations

$$\nabla \cdot \mathbf{u} = 0 \tag{1}$$

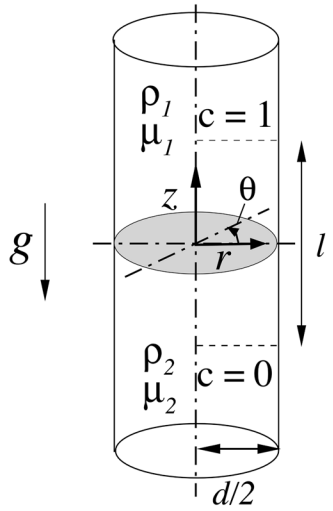

FIGURE 1. Sketch of the vertical capillary tube and the cylindrical coordinate system.

$$\nabla p = \nabla \cdot \underline{\tau} + \rho g \mathbf{e_g} \tag{2}$$

$$\frac{\partial c}{\partial t} + \mathbf{u} \cdot \nabla c = D \nabla^2 c. \tag{3}$$

These equations describe the conservation of mass, momentum, and species, respectively. Here **u** represents the flow velocity, the gravitational acceleration g points in the $-z$-direction given by unit vector $\mathbf{e_g}$, c indicates the concentration of the heavier fluid, $\underline{\tau}$ denotes the viscous stress tensor, and D represents the diffusion coefficient, which is assumed constant. Note that implicitly contained in the above set of equations is the Boussinesq approximation, which assumes that density variations are significant in the gravitational term only.

Following other authors, the density ρ and the viscosity μ are assumed to be linear and exponential functions of the concentration c, respectively,

$$\rho = \rho_2 + c(\rho_1 - \rho_2) \tag{4}$$

$$\mu = \mu_2 e^{Rc}, \tag{5}$$

where ρ_1 and μ_1 indicate the density and viscosity of the heavier fluid, and ρ_2 and μ_2 represent the counterparts for the lighter fluid. The mobility ratio R is given by

$$R = \ln \frac{\mu_1}{\mu_2}. \tag{6}$$

The governing equations are rendered dimensionless by introducing a characteristic length L^*, velocity U^*, time T^*, pressure P^*, and density difference G^* in the form

$$L^* = d \tag{7}$$

$$U^* = \frac{\Delta \rho g d^2}{\mu_{\min}} \tag{8}$$

$$T^* = \frac{\mu_{\min}}{\Delta \rho g d} \tag{9}$$

$$P^* = \Delta \rho g d \tag{10}$$

$$R^* = \Delta \rho = \rho_1 - \rho_2. \tag{11}$$

Note that the nondimensionalization is always carried out with the smaller viscosity, so that a meaningful comparison can be made between cases in which either the lighter or the heavier fluid is the more viscous.

$$\nabla \cdot \mathbf{u} = 0 \tag{12}$$

$$\nabla p = \nabla \cdot \underline{\tau} - c \mathbf{e_g} \tag{13}$$

$$\frac{\partial c}{\partial t} + \mathbf{u} \cdot \nabla c = \frac{1}{Ra} \nabla^2 c, \tag{14}$$

where the Rayleigh number Ra is defined by

$$Ra = \frac{\Delta \rho g d^3}{D \mu_{\min}}. \tag{15}$$

The Stokes equations, when formulated in cylindrical coordinates (r, θ, z), exhibit terms of the form r^{-1}, r^{-2}, r^{-3}, which lead to geometric singularities at the axis, $r = 0$. Verzicco and Orlandi[20] proposed rewriting the governing equations by replacing the velocity components v_r, v_θ, and v_z by $q_r = v_r \cdot r$, $q_\theta = v_\theta$, and $q_z = v_z$, respectively. Thus, by definition $q_r = 0$ on the axis, which on a staggered grid avoids the problem of singularities. The authors also demonstrate that alternative formulations (e.g., $q_\theta = v_q \cdot r$) neither enhance the accuracy nor simplify the discretization. Hence, we used this formulation for our numerical analysis.

LINEAR STABILITY ANALYSIS

Linearization and Formulation of the Eigenvalue Problem

We linearize the above set of equations around a quiescent base state

$$\begin{bmatrix} q_r \\ q_\theta \\ q_z \\ p \\ c \end{bmatrix}(r, \theta, z, t) = \begin{bmatrix} 0 \\ 0 \\ 0 \\ \bar{p} \\ \bar{c} \end{bmatrix}(z) + \begin{bmatrix} q_r' \\ q_\theta' \\ q_z' \\ p' \\ c' \end{bmatrix}(r, \theta, z, t), \tag{16}$$

where the base concentration profile is given by

$$\bar{c} = 0.5 + 0.5 \cdot \mathrm{erf}\left(\frac{z}{\delta}\right). \tag{17}$$

The parameter δ denotes the thickness of the interfacial region. We assume that the diffusive time scale of the base state is much larger than the characteristic time scale of the instability growth, so that the base state can be held constant for the purpose of evaluating the instability growth rate. The perturbations, denoted by a prime, are assumed to have the form

$$\begin{bmatrix} q_r' \\ q_\theta' \\ q_z' \\ p' \\ c' \end{bmatrix}(r, \theta, z, t) = \begin{bmatrix} \hat{q}_r(r, z) \cdot \cos(\beta\theta) \\ \hat{q}_\theta(r, z) \cdot \sin(\beta\theta) \\ \hat{q}_z(r, z) \cdot \cos(\beta\theta) \\ \hat{p}(r, z) \cdot \cos(\beta\theta) \\ \hat{c}(r, z) \cdot \cos(\beta\theta) \end{bmatrix} e^{\sigma t}, \tag{18}$$

where the "hatted" quantities represent axisymmetric eigenfunctions and β denotes the azimuthal wave number. It should be noted that, due to the underlying geometry of the problem, only integral values of β have physical significance. By substituting the above relations into the dimensionless conservation equations, subtracting out the base state and linearizing, we obtain the system of linear equations in terms of q_r, q_θ and q_z as

$$0 = \frac{\partial \hat{q}_r}{\partial r} + \beta \hat{q}_\theta + r\frac{\partial \hat{q}_z}{\partial z} \tag{19}$$

$$\frac{\partial \hat{p}}{\partial r} = e^{R\bar{c}}\left[\frac{\partial}{\partial r}\left(\frac{1}{r}\frac{\partial \hat{q}_r}{\partial r}\right) - \frac{\beta^2}{r^3}\hat{q}_r + \frac{1}{r}\frac{\partial^2 \hat{q}_r}{\partial z^2} - \frac{2\beta}{r^2}\hat{q}_\theta + R\frac{\partial \bar{c}}{\partial z}\frac{\partial \hat{q}_z}{\partial r} + R\frac{1}{r}\frac{\partial \bar{c}}{\partial z}\frac{\partial \hat{q}_r}{\partial z}\right] \quad \textbf{(20)}$$

$$-\frac{1}{r}\beta\hat{p} = e^{R\bar{c}}\left[\frac{\partial}{\partial r}\left(\frac{1}{r}\frac{\partial}{\partial r}(r\hat{q}_\theta)\right) - \frac{\beta^2}{r^2}\hat{q}_\theta + \frac{\partial^2 \hat{q}_\theta}{\partial z^2} - \frac{2\beta}{r^3}\hat{q}_r + R\frac{\partial \bar{c}}{\partial z}\frac{\partial \hat{q}_\theta}{\partial z} - R\frac{\beta}{r}\frac{\partial \bar{c}}{\partial z}\hat{q}_z\right] \quad \textbf{(21)}$$

$$\frac{\partial \hat{p}}{\partial z} = e^{R\bar{c}}\left[\frac{1}{r}\frac{\partial}{\partial r}\left(r\frac{\partial \hat{q}_z}{\partial r}\right) - \frac{\beta^2}{r^2}\hat{q}_z + \frac{\partial^2 \hat{q}_z}{\partial z^2} + 2R\frac{1}{r}\frac{\partial \bar{c}}{\partial z}\frac{\partial \hat{q}_z}{\partial z}\right] - \hat{c} \quad \textbf{(22)}$$

$$\sigma\hat{c} + \frac{\partial \bar{c}}{\partial z}\hat{q}_z = \frac{1}{Ra}\left[\frac{\partial^2 \hat{c}}{\partial r^2} + \frac{1}{r}\frac{\partial \hat{c}}{\partial r} - \frac{\beta^2}{r^2}\hat{c} + \frac{\partial^2 \hat{c}}{\partial z^2}\right]. \quad \textbf{(23)}$$

This represents an eigenvalue problem with $\hat{p}$, $\hat{q}_r$, $\hat{q}_\theta$, $\hat{q}_z$, and $\hat{c}$ as eigenfunctions and σ as the eigenvalue of the system. There are three externally prescribed parameters in the form of the Rayleigh number Ra, the mobility ratio R, and the initial interfacial thickness δ.

NUMERICAL IMPLEMENTATION AND BOUNDARY CONDITIONS

The computation domain for the solution of the eigenvalue problem extends from the axis to the outer wall in the r-direction, that is, from 0 to 0.5, and from $-l/2$ to $l/2$ in the vertical z-direction, as shown in FIGURE 1. The domain length l has to be chosen sufficiently large for its effect on the numerical eigenvalue and eigenfunction results to be negligible.

Three-Dimensional Perturbations

The linear equations **(20)**–**(23)** are discretized by second order finite differences in both the r- and z-directions. To concentrate the numerical resolution in the interfacial region, a non-equidistant grid is taken such that an appropriate concentration of grid points is obtained in the interfacial region. The required numerical resolution is established by means of test calculations. These show that for most cases $N_r = 19$ points in the radial direction is sufficient to keep the error in the eigenvalue to less than 0.1%. The required number of points in the z-direction depends on the domain length and the interface thickness δ. The largest calculations employ up to $N_z = 91$ and $N_r = 23$ points, which results in a matrix of size $5N_zN_r \times 5N_zN_r = 10{,}465 \times 10{,}465$.

At the outer wall of the tube (i.e., at $r = 0.5$), all velocity components are assumed to vanish, as well as the normal derivative of the concentration perturbation. The vertical domain boundaries are sufficiently far away from the interface that we can prescribe homogeneous Dirichlet conditions for all velocity components, as well as for the concentration perturbation. At the axis $r = 0$, $q_r = 0$ since $q_r = v_r \cdot r$. We do not need to specify boundary conditions for the other velocity components or the concentration perturbation, at the axis, since the use of staggered grid implies that only grid points for the radial velocity lie on the axis. For the pressure variable, no boundary conditions are necessary, because we employ a staggered grid.

Axisymmetric Perturbations

To obtain information on the stability of purely axisymmetric perturbations, we consider the case $\beta = 0$ separately. This provides an additional validation of the three-dimensional approach in the limit of small wave numbers. To avoid boundary conditions for pressure and also to save memory by reducing the total number of variables used in the computation, we conveniently rewrite the governing equations in the stream function and vorticity variables.

Vorticity ω and stream function ψ are defined, as usual by

$$v_r = -\frac{1}{r}\frac{\partial \psi}{\partial z}, \qquad v_z = \frac{1}{r}\frac{\partial \psi}{\partial r} \tag{24}$$

$$\omega = \frac{\partial v_r}{\partial z} - \frac{\partial v_z}{\partial r}. \tag{25}$$

We assume an axisymmetric disturbance of the form

$$\begin{bmatrix} \psi' \\ \omega' \\ c' \end{bmatrix}(r, z, t) = \begin{bmatrix} \hat{\psi}(r, z) \\ \hat{\omega}(r, z) \\ \hat{c}(r, z) \end{bmatrix} e^{\sigma t}. \tag{26}$$

Using these relations and linearizing, similar to the three-dimensional case, we obtain the system of linear equations

$$0 = \nabla^2 \hat{\psi} + \hat{\omega} \tag{27}$$

$$\begin{aligned} 0 = {} & \nabla^2 \hat{\omega} + 2R\frac{\partial \bar{c}}{\partial z}\frac{\partial \hat{\omega}}{\partial z} + \left(\frac{\partial \bar{c}}{\partial z}\right)^2 \hat{\omega} + R^2 \frac{\partial^2 \bar{c}}{\partial z^2}\hat{\omega} - 2R^2 \frac{1}{r^2}\left(\frac{\partial \bar{c}}{\partial z}\right)^2 \frac{\partial \hat{\psi}}{\partial r} \\ & - \frac{2R}{r^2}\frac{\partial^2 \bar{c}}{\partial z^2}\frac{\partial \hat{\psi}}{\partial r} - \frac{2R}{r}\frac{\partial \bar{c}}{\partial z}\frac{\partial^3 \hat{\psi}}{\partial z} + e^{-R\bar{c}}\frac{\partial \hat{c}}{\partial r} \end{aligned} \tag{28}$$

$$\sigma \bar{c} = \frac{1}{Ra}\nabla^2 \hat{c} - \frac{1}{r}\frac{\partial \bar{c}}{\partial z}\frac{\partial \hat{\psi}}{\partial r}, \tag{29}$$

where $\hat{\psi}$ is set to zero on all domain boundaries and $\hat{\omega}$ vanishes on all boundaries except for the outer wall, where it takes the value $(1/r)(\partial^2 \hat{\psi}/\partial r^2)$. At the far-field boundaries the concentration perturbation is assumed to vanish, whereas along the outer wall and the tube axis its normal derivative $\partial \hat{c}/\partial r$ tends to zero. A staggered grid is not required here due to the absence of the pressure variable and of singularities at the axis. Hence, a Chebyshev collocation method is used in the z-direction with two separate subdomains that cover the regions $z \geq 0$ and $z \leq 0$, respectively, in order to concentrate grid points at the interface. In the radial direction a highly accurate, compact finite difference scheme of third order at the wall and up to tenth order in the interior is used.[21] More details about the numerical implementation are published elsewhere.[22]

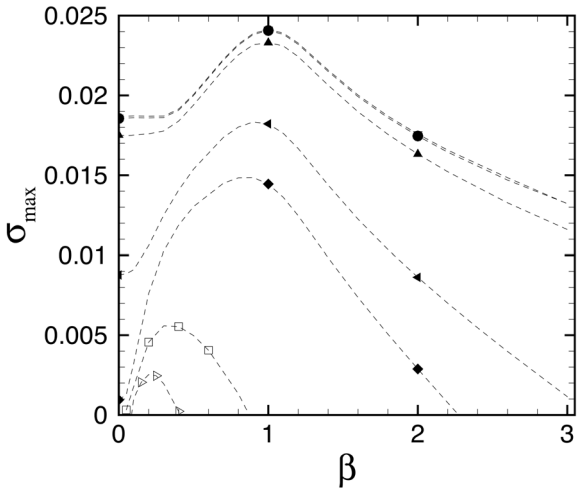

FIGURE 2. Three-dimensional perturbations, dispersion relationships for $\delta = 0.1$ and *Ra* values: ▷, 5×10^2; □, 10^3; ◆, 5×10^3; ◀, 10^4; ▲, 10^5; ●, 10^6; ▼, 10^7. For comparison, the axisymmetric data are plotted as well. The growth rate for $\beta = 1$ is seen to exceed that for $\beta = 0$ for all values of *Ra*.

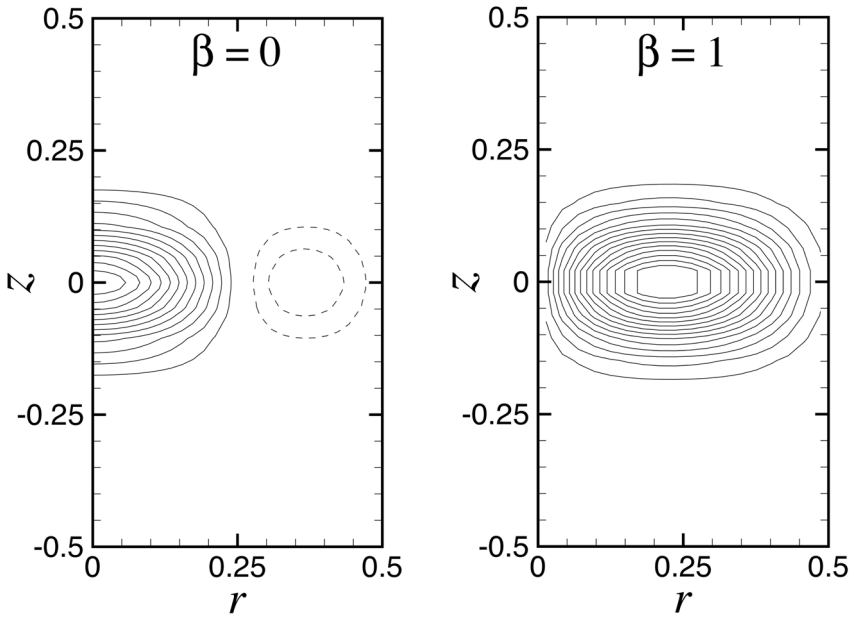

FIGURE 3. Isocontours of the concentration eigenfunction $\hat{c}$ for $\beta = 0$ and 1 for $\delta = 0.1$ and $Ra = 10^5$.

RESULTS

Constant Viscosity

In FIGURE 2 the leading eigenvalue is plotted as a function of the wave number β for several *Ra* values, ranging from 500 to 10^7, and a constant thickness of the interface $\delta = 0.1$. These dispersion relationships show that for small and intermediate wave numbers, the curves for $Ra > 10^6$ become indistinguishable, implying that an additional increase in *Ra* affects only the range of unstable wave numbers and the short-wavelength cutoff, but not the most dangerous wave number or its growth rate. It should be noted that the data for noninteger values of β are plotted in FIGURE 2 to guide the eye, because only the integer values are of physical significance. FIGURE 2 demonstrates that the azimuthal perturbation $\beta = 1$ is always more unstable than its axisymmetric counterpart. The concentration eigenfunctions for $\beta = 0$ and 1 are shown in FIGURE 3 for $\delta = 0.1$ and $Ra = 10^5$. The presence of only one sign in the eigenfunction for $\beta = 1$ indicates that the lighter fluid is rising in one half of the capillary tube, with the heavier fluid sinking in the other half. The qualitative form of the fingers produced is illustrated in FIGURE 4.

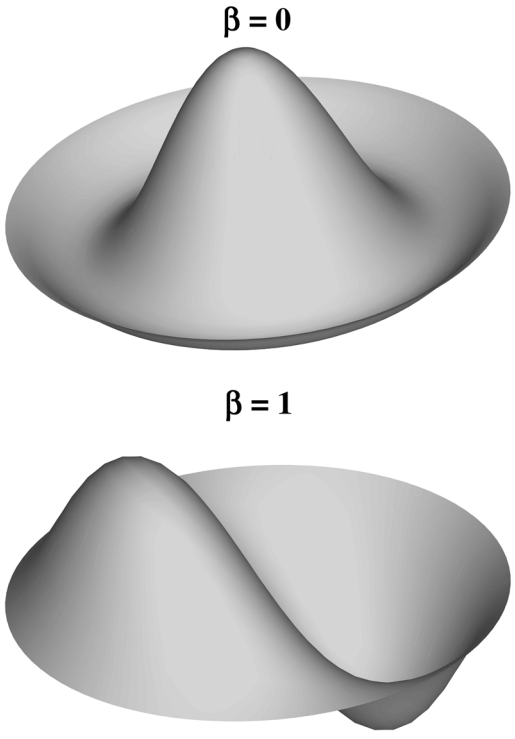

FIGURE 4. Qualitative form of finite amplitude fingers for $\delta = 0.1$ and $Ra = 10^7$.

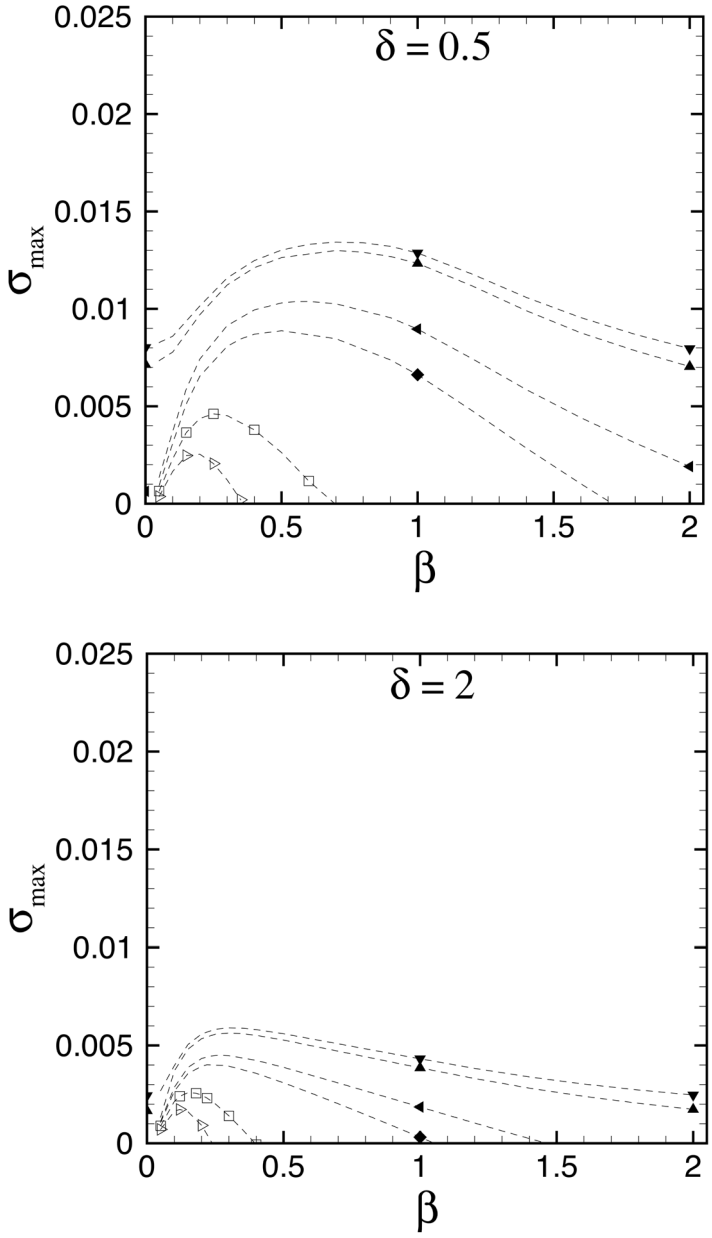

FIGURE 5. Dispersion relationships for various interface thickness values and Rayleigh numbers: ▷, 5×10^2; □, 10^3; ◆, 5×10^3; ◀, 10^4; ▲, 10^5; ▼, 10^7. $\beta = 1$ represents the most amplified integer mode for all values of δ and *Ra*.

For larger values of δ, the corresponding dispersion relationships are presented in FIGURE 5. We observe a general trend of decreasing growth rate and smaller cutoff wave number for increasing interface thickness. However, there is no qualitative change in the shape of the concentration eigenfunction $\hat{c}$ with increasing thickness, as is shown in FIGURE 6. From the dispersion relationships shown in FIGURES 2 and 5 we deduce that for all values of the interface thickness, $\beta = 1$ remains the most dangerous mode. For this reason, we consider this wave number in more detail.

By extrapolating the growth rate for $\beta = 1$ and $Ra = 10^7$ to $\delta = 0$, we find that the maximum eigenvalue for a step-like concentration base state is approximately 0.028, as shown in FIGURE 7. The variation of the growth rate σ with Ra, for various δ values and $\beta = 1$, is shown in FIGURE 8. In general, thinner interfaces and larger Ra values are seen to be destabilizing. For $Ra > 10^6$, the growth rate is seen to asymptotically reach a plateau, the value of which depends on δ.

For each δ, a critical value Ra_{crit} can be identified below which the base state is stable to axisymmetric perturbations. The existence of this critical value reflects the stabilizing influence of the outer wall. The Ra_{crit} values found here for capillary tubes are significantly higher than those reported elsewhere[17] for Hele–Shaw cells. This is to be expected, since the stabilizing influence by the walls should be stronger in a capillary tube, where the perturbation is surrounded by the solid wall on all sides. In a Hele–Shaw cell, on the other hand, the perturbations are affected by the walls only in the direction normal to the gap, but not in the spanwise direction. FIGURE 9 depicts the critical Rayleigh number Ra_{crit} as a function of δ, for $\beta = 1$ and $\beta = 0$. For all interface thicknesses, the value of Ra_{crit} for $\beta = 1$ is smaller than the corresponding value for $\beta = 0$. By linear regression through the data points for $\beta = 1$, we obtain the relationship

$$Ra_{\mathrm{crit}} = 1800\delta + 920. \tag{30}$$

This relationship indicates that Rayleigh numbers below $O(920)$ are stable for all base concentration profiles, with respect to any axisymmetric or three-dimensional perturbation.

It is interesting to compare the above relationship **(30)** for the present, error function type base concentration profiles with the classical result[2] dealing with unstable density stratifications with a constant gradient dc/dz in a capillary tube. Taylor demonstrated that such profiles are stable as long as

$$\frac{\dfrac{dc}{dz}\rho_0 g \alpha d^4}{D\mu} \leq 1087, \tag{31}$$

where

$$\rho = \rho_0(1 + \alpha c). \tag{32}$$

For relatively smooth base concentration profiles of the error function type (i.e., reasonably large values of δ) the present criterion **(30)** should approach the classical Taylor criterion **(31)**. To check if this is the case, we rewrite **(30)** for dimensional δ as

$$\left(d\frac{dc}{dz}\right)^{-1} \times \frac{\dfrac{dc}{dz}\rho_0 g \alpha d^4}{D\mu} \leq 1800\frac{\delta}{d} + 920. \tag{33}$$

In the first term on the left hand side, we approximate dc/dz by the value at $z = 0$

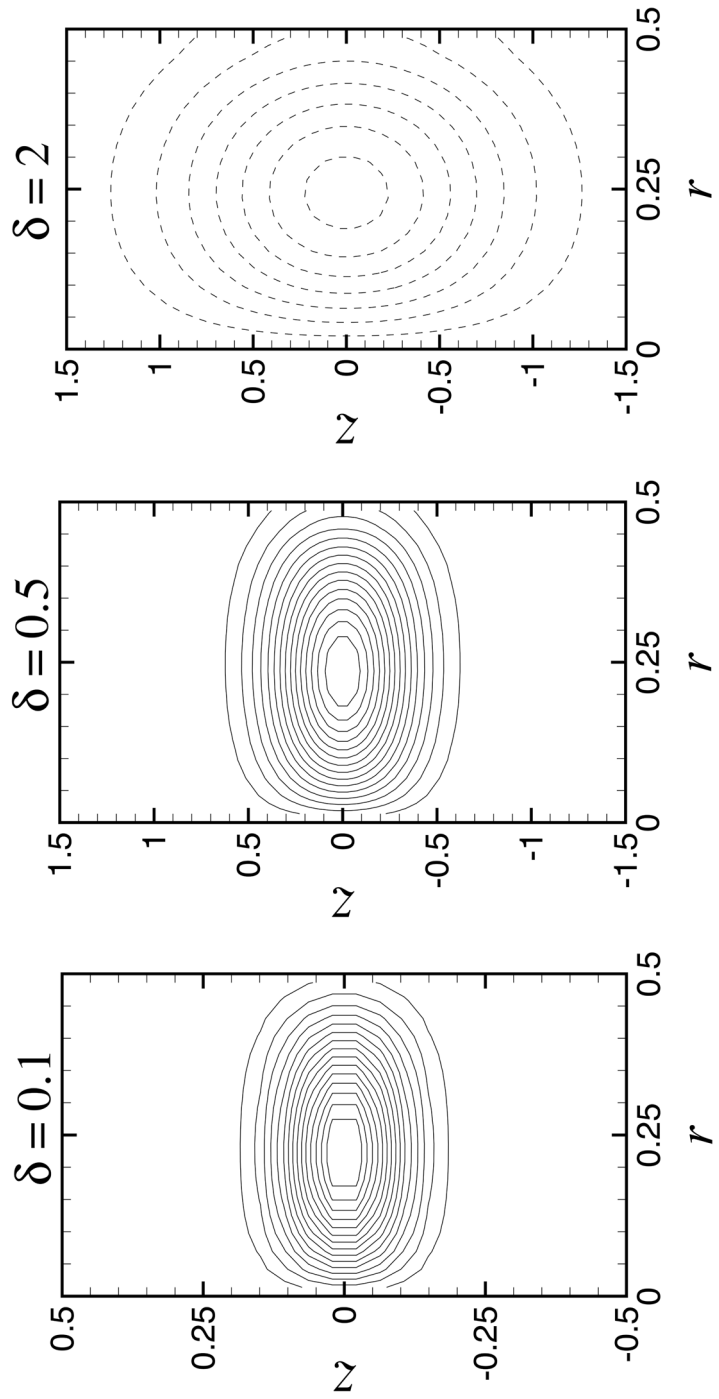

FIGURE 6. Isocontours of the concentration eigenfunction $\hat{c}$ for various values of δ, at $Ra = 10^5$ and $\beta = 1$. Although the isocontours become flatter for decreasing δ, their shapes remain qualitative the same.

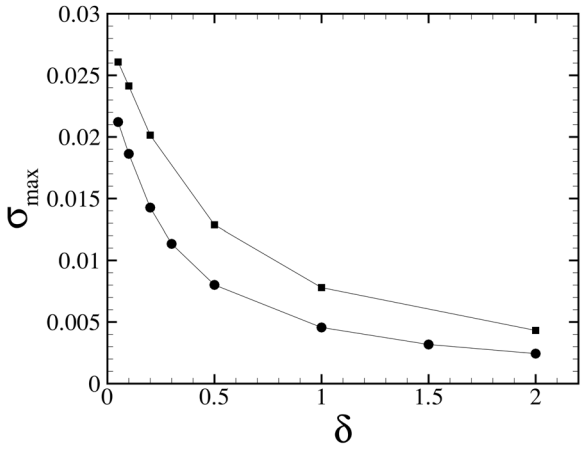

FIGURE 7. The growth rate σ as a function of δ, for β = 0 (●) and β = 1 (■), with $Ra = 10^7$. This indicates that for all values of the interface thickness, β = 1 remains more dangerous than the axisymmetric mode.

$$\left.\frac{dc}{dz}\right|_{z=0} = \frac{1}{\delta\sqrt{\pi}}. \tag{34}$$

For $\delta/d = 2$, we thus obtain

$$\frac{\frac{dc}{dz}\rho_0 g\alpha d^4}{D\mu} \leq 1275, \tag{35}$$

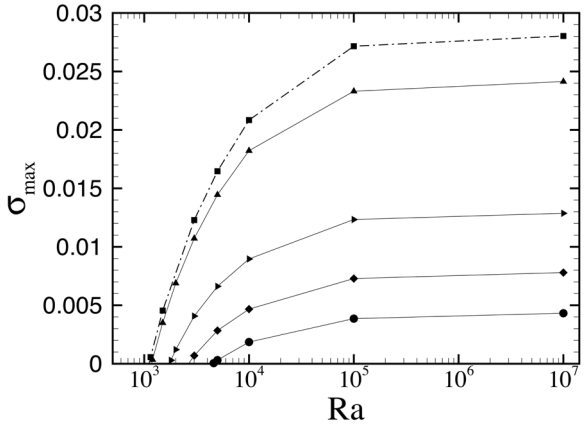

FIGURE 8. The growth rate σ corresponding to the most dangerous wave number β = 1 as a function of *Ra* for interface thickness δ: ■, 0; ▲, 0.1; ▶, 0.5; ◆, 1; ●, 2. The *dashed line* corresponds to extrapolated data for the step function profile.

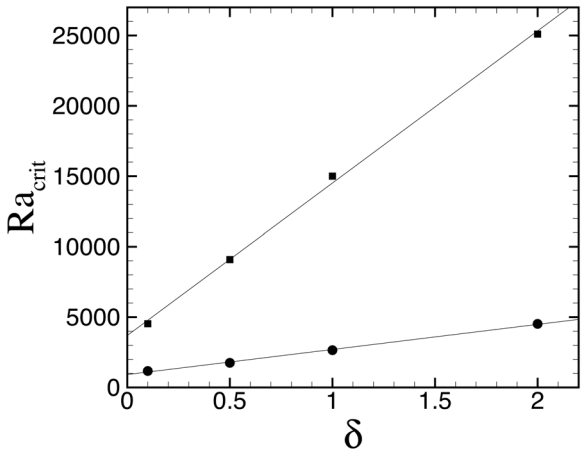

FIGURE 9. The critical Rayleigh number Ra_{crit} as a function of the interfacial thickness parameter δ, for the axisymmetric mode $\beta = 0$ (■) and the most dangerous three-dimensional mode $\beta = 1$ (●). For all values of δ, the axisymmetric mode is seen to have a larger value of Ra_{crit}.

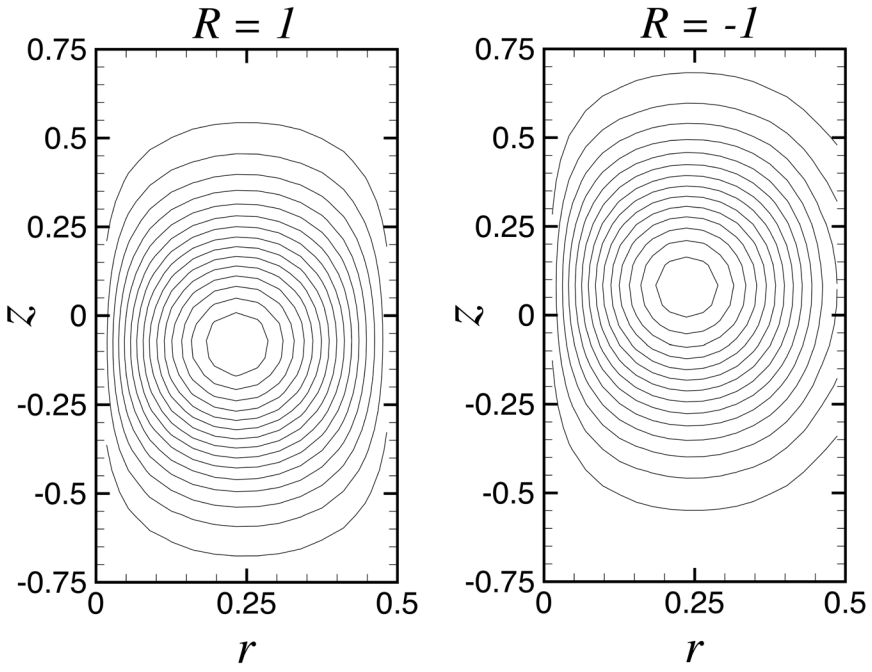

FIGURE 10. Isocontours of the concentration eigenfunction $\hat{c}$ for $R = 1$ and $R = -1$ for $\delta = 0.5$, $\beta = 1$, and $Ra = 10^5$. The eigenvalue corresponding to both cases is $\sigma = 7.97 \times 10^{-3}$. The maxima of the eigenfunctions are always shifted toward the less viscous fluid.

which is indeed close to the relationship, **(31)**, derived by Taylor. The slightly higher value than Taylor's result is expected, since we based the comparison on the largest value of the concentration gradient, rather than its average value.

Variable Viscosity

FIGURE 10 shows the concentration eigenfunction contours for $R = 1$ (less viscous fluid below) and $R = -1$ (less viscous fluid above). Although the growth rates are identical, the maxima of the eigenfunctions are shifted in opposite directions; that is, always toward the less viscous fluid. It has been demonstrated[18] that a simple transformation of the governing equations (Stokes equations) shows the eigenvalues to be equal for both the cases. As a consequence we limit our discussion to positive values of the mobility ratio.

FIGURE 11 displays the dispersion relations for $\delta = 0.1$, $Ra = 10^7$, and various values of the mobility ratio R. An increase in the mobility ratio R dampens the growth of the instability, due to the higher average viscosity of the two-fluid system. However, FIGURE 12 shows a crossover of the most unstable mode from azimuthal to axisymmetric for large values of R and $Ra > 10^5$. Hence the damping influence, with increasing mobility ratio, is much stronger on the three-dimensional mode than the corresponding axisymmetric mode for large Rayleigh numbers. However, no such change of stability occurs for lower Rayleigh numbers, because all the unstable modes in this case are equally damped.

For a constant mobility ratio, similar to the constant viscosity case, the growth rate increases with the Rayleigh number, until it reaches a plateau at about $Ra = 10^5$. Furthermore, the eigenfunctions and finger shapes are similar to the constant viscosity case (cf. FIGS. 3 and 10) except that they are no longer symmetric but shifted toward the less viscous fluid.

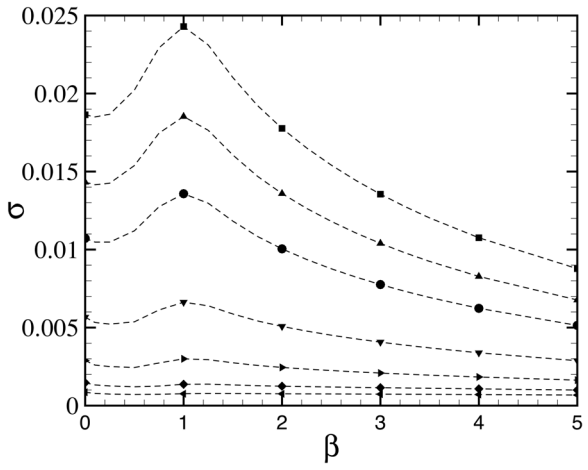

FIGURE 11. Growth rate as a function of β for various mobility ratios R: ■, 0; ▲, 0.5; ●, 1; ▼, 2; ▶, 3; ◆, 4; ◀, 5 with $\delta = 0.1$ and $Ra = 10^7$. Increasing the mobility ratio has a stabilizing effect.

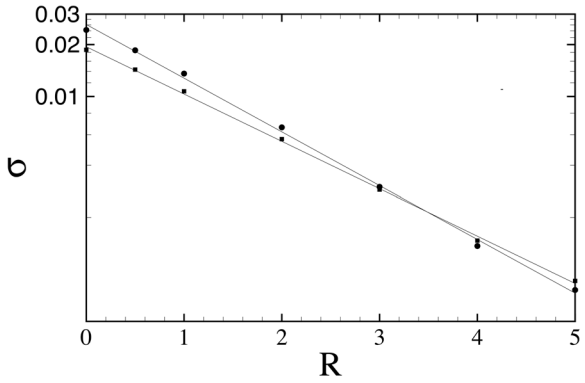

FIGURE 12. Non-uniform damping with increasing mobility ratio results in a crossover of the most unstable mode from $\beta = 1$ (●) to $\beta = 0$ (■). For $\delta = 0.1$ and $Ra = 10^7$, crossover occurs at $R = 3.48$.

FIGURE 13 shows the variation of the maximum growth rate with the interface thickness for $\beta = 0$ and $\beta = 1$, at two different values of the mobility ratio. We find that for larger mobility ratios the highest growth rates occur at an intermediate value of the interfacial thickness. This is in contrast to the constant viscosity case, for which the growth rate is seen to decline monotonically with increasing interface thickness (compare with FIGS. 2 and 5). FIGURE 13 also shows that the most unstable interface thickness increases with the mobility ratio.

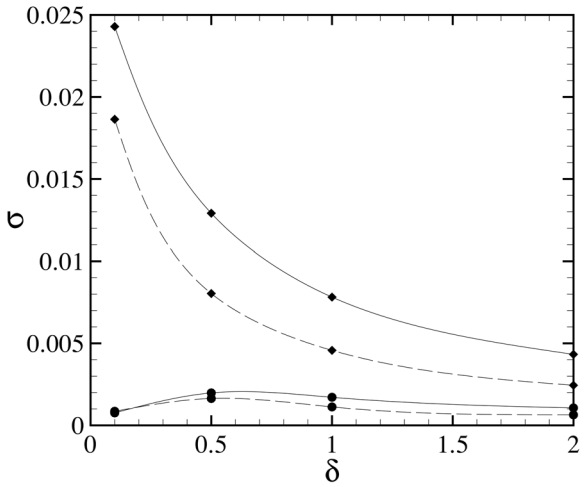

FIGURE 13. The growth rate σ as a function of δ for -◆-, $R = 0$, $\beta = 0$; —◆—, $R = 0$, $\beta = 0$; -●-, $R = 0$, $\beta = 0$; —●—, $R = 0$, $\beta = 0$. In all cases $Ra = 10^7$. For larger mobility ratios, interfaces with intermediate thicknesses are seen to be most unstable.

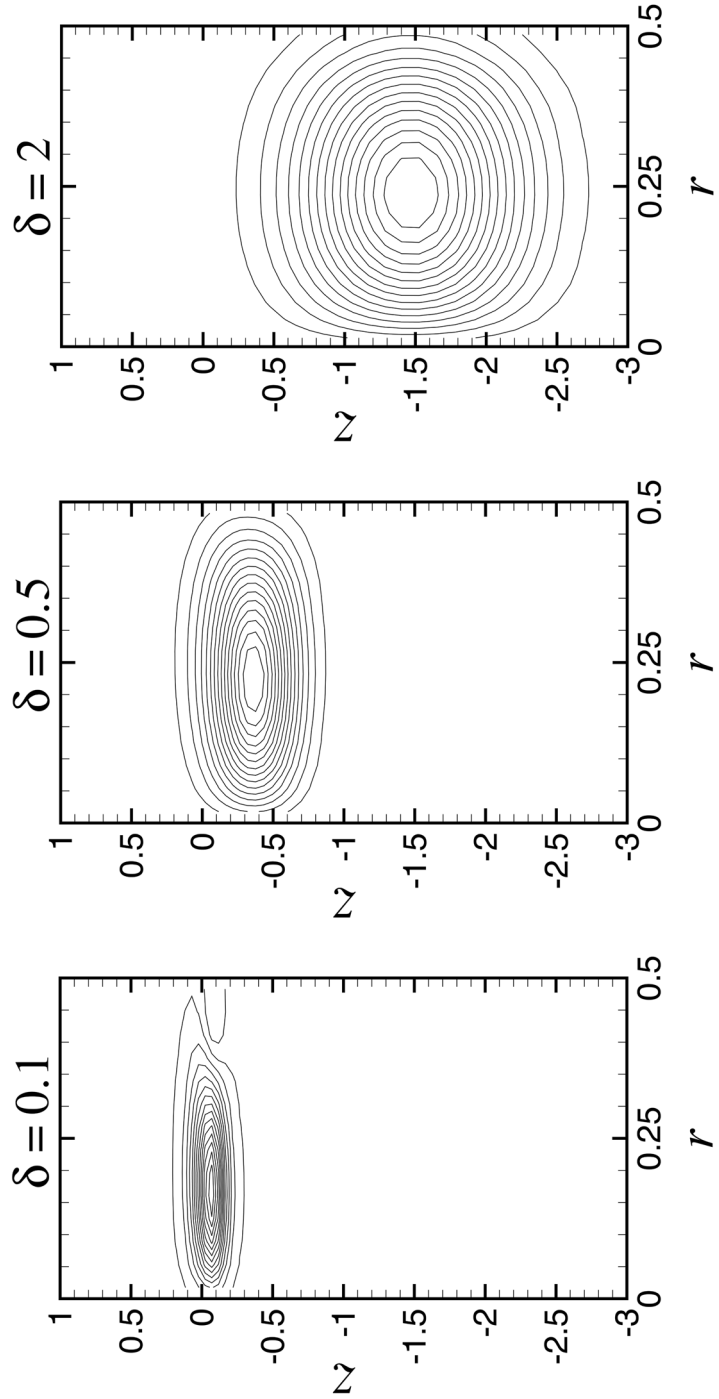

FIGURE 14. Concentration eigenfunctions of the most amplified mode for $Ra = 10^6$, $R = 5$ and different values of δ. For thicker interfaces, the perturbation is located almost entirely in the less viscous fluid.

TABLE 1. Concentration gradient and fluid viscosity at the location of the eigenfunction maximum for $Ra = 10^6$ and $R = 5$

δ	$\bar{c}_z/(\bar{c}_z)_{max}$	μ/μ_{min}
0.1	0.61	2.583
0.5	0.56	2.035

The shapes of the eigenfunctions shown in FIGURE 14 explain the emergence of this most unstable interface thickness. We note that the vertical extent of the eigenfunctions is affected by *both* of the two externally imposed length scales, namely, the tube diameter and the interface thickness. Due to this influence of the tube diameter, for interface thicknesses much smaller than the tube diameter, the vertical scale of the eigenfunction does not decrease at the same rate as δ. Conversely, for interface thicknesses larger than the tube diameter, the size of the eigenfunction does not increase as strongly with δ. As a result, for thin interfaces the eigenfunction extends over a region several times wider than the interface. Since it has to be anchored in the region of the unstable density gradient, it has to extend substantially into the high viscosity fluid, which exerts a stabilizing influence. In contrast, for thick interfaces the eigenfunction can reside almost entirely within the interfacial region, so that its maximum can shift substantially toward the low viscosity region. In other words, the eigenfunction can select a location that represents an optimal combination of unstable density gradient and low viscosity fluid. This is confirmed by TABLE 1, which provides a comparison of the normalized density gradient and the viscosity for two values of δ. The table shows that for the thicker interface the normalized concentration gradient, and hence, the driving force behind the instability, has not decreased much, but the fluid viscosity at the location of the eigenfunction maximum shows that its completely in the lower viscosity fluid for $\delta = 0.5$. Hence, the thicker interface gives rise to a stronger overall instability.

CONCLUSIONS

The current investigation presents linear stability results for the miscible interface formed by placing a heavier fluid above a lighter fluid, with different viscosities, in a vertically oriented capillary tube. The analysis is based on the three-dimensional Stokes equations coupled to a convection–diffusion equation for the concentration field in cylindrical coordinates. By linearizing this set of equations, a generalized eigenvalue problem is formulated, whose numerical solution yields both the growth rate as well as the two-dimensional eigenmodes as functions of the dimensionless parameters characterizing the problem; namely, the Rayleigh number, the mobility ratio, and the interface thickness.

For constant viscosity case, the dispersion relations show that for all *Ra* values and interface thicknesses the azimuthal mode $\beta = 1$ represents the most unstable disturbance. In particular, its growth rates are consistently higher than those of the axisymmetric mode. The most amplified mode thus corresponds to the formation of one finger of the lighter fluid rising over one half of the tube cross section, with a second finger of the heavier fluid falling in the other half. This is in agreement with other

experimental observations.[16] The stability results, furthermore, indicate the existence of a critical Rayleigh number $Ra_{crit} \approx 920$, below which all perturbations are stable. For relatively thick interfaces, the present data for Ra_{crit} are seen to approach the classical value[2] for a uniform density gradient. For a constant interface thickness, the growth rates reach a plateau as $Ra > 10^6$. The detailed numerical analysis for density-driven instability of identical viscosity miscible fluids is given elsewhere.[22]

When the viscosity of either fluid is increased, the instability is damped compared to the constant viscosity case. There is a crossover of the most unstable mode from azimuthal to axisymmetric for large values of R and $Ra > 10^5$. Hence, the damping influence, with variable viscosity, is much stronger on the three-dimensional mode than the corresponding axisymmetric mode for large Rayleigh numbers. It is also seen that the growth rate does not depend on which of the two fluids is the more viscous. For every parameter combination the maximum of the eigenfunctions tends to shift toward the less viscous fluid. For a fixed mobility ratio, similar to the constant viscosity case, the growth rates are seen to reach a plateau for Rayleigh numbers in excess of 10^6. An interesting observation is that at higher mobility ratios the largest growth rates and unstable wave numbers are obtained for intermediate interface thicknesses. Thus, with different viscosity fluids, thicker interfaces can be more unstable than their thinner counterparts.

Other experiments[16] had shown that a small amount of net flow through the capillary tube can stabilize the azimuthal instability mode and maintain an axisymmetric evolution of the flow. To analyze the effect of a net flow onto the linear stability of the interface, we need to include a base flow of Poiseuille type in our analysis. Efforts in this direction are currently underway.

ACKNOWLEDGMENTS

We thank Professors Tony Maxworthy and Bud Homsy for helpful discussions. Support for this research was received from the NASA Microgravity and NSF/ITR programs, as well as from the Department of Energy, the UC Energy Institute, and through an NSF equipment grant.

REFERENCES

1. HALES, A. 1937. Convection currents in geysers. Mon. Not. R. Astron. Soc., Geophys, Suppl. **4:** 122.
2. TAYLOR, G. 1954. Diffusion and mass transport in tubes. Proc. Roy. Soc. B **67:** 857.
3. DEBACQ, M., V. FANGUET, J HULIN & D. SALIN. 2001. Self-similar concentration profiles in buoyant mixing of miscible fluids in a vertical tube. Phys. Fluids **13:** 3097.
4. WOODING, R. 1959. The stability of a viscous liquid in a vertical tube containing porous material. Proc. Roy. Soc. A **252:** 120.
5. BATCHELOR, G. & J. NITSCHE. 1993. Instability of stratified fluid in a vertical cylinder. J. Fluid Mech. **252:** 419.
6. TAYLOR, G. 1960. Deposition of a viscous fluid on the wall of a tube. J. Fluid Mech. **10:** 161.
7. COX, B. 1962. On driving a viscous fluid out of a tube. J. Fluid Mech. **14:** 81.
8. REINELT, D. & P. SAFFMAN. 1985. The penetration of a finger into a viscous fluid in a channel and tube. SIAM J. Sci. Statist. Comput. **6:** 542.

9. SOARES, E., M. CARVALHO & P.S. MENDES. 2004. Immiscible liquid-liquid displacement in capillary tubes. J. Fluid Mech. Submitted.
10. PETITJEANS, P. & T. MAXWORTHY. 1996. Miscible displacements in capillary tubes. Part 1. experiments. J. Fluid Mech. **326:** 37.
11. CHEN, C. & E. MEIBURG. 1996. Miscible displacements in capillary tubes. Part 2. numerical simulations. J. Fluid Mech. **326:** 57.
12. SCOFFONI, J., E. LAJEUNESSE & G. HOMSY. 2000. Interface instabilities during displacements of two miscible fluids in a vertical pipe. Phys. Fluids **13**(3): 553.
13. KORTEWEG, D. 1901. Sur la forme que prennent les équations du mouvement des fluides si l'on tient compte des forces capillaires causées par des variations de densité. Arch. Neel. Sci. Ex. Nat. **II:** 6.
14. JOSEPH, D. & Y. RENARDY. 1992. Fundamentals of Two-Fluid Dynamics. Springer-Verlag, New York.
15. CHEN, C. & E. MEIBURG. 2002. Miscible displacements in capillary tubes: influence of korteweg stresses and divergence effects. Phys. Fluids **14**(7): 2052.
16. KUANG, J., T. MAXWORTHY & P. PETITJEANS. 2003. Miscible displacements between silicone oils in capillary tubes. Eur. J. Mech. B/Fluids **22:** 271–277.
17. GRAF, F., E. MEIBURG & C. HÄRTEL. 2002. Density-driven instabilities of miscible fluids in a hele-shaw cell: linear stability analysis of the three-dimensional stokes equations. J. Fluid Mech. **451:** 261.
18. GOYAL, N. & E. MEIBURG. 2004. Unstable density stratification of miscible fluids in a verical hele-shaw cell: influence of variable viscosity on the linear stability analysis. J. Fluid Mech. **516:** 211.
19. FERNANDEZ, J., P. KUROWSKI, P. PETITJEANS & E. MEIBURG. 2002. Density-driven, unstable flows of miscible fluids in a hele-shaw cell. J. Fluid Mech. **451:** 239.
20. VERZICCO, R. & P. ORLANDI. 1996. A finite-difference scheme for three-dimensional incompressible flows in cylinder coordinates deposition of a viscous fluid on the wall of a tube. J. Comp. Phys. **123:** 402.
21. LELE, S. 1992. Compact finite difference schemes with spectral-like resolution. J. Comp. Phys. **103:** 16.
22. VANAPARTHY, S., E. MEIBURG & D. WILHELM. 2003. Density driven instabilities of miscible fluids in a capillary tube: linear stability analysis. J. Fluid Mech. **497:** 99.